

Asymptotic Performance of TDOA Estimation using Satellites

Hodaya Halevi, *Student Member, IEEE*, Itsik Bergel, *Senior Member, IEEE* and Yair Noam, *Member, IEEE*

Abstract—We present novel lower bounds on the localization error using a network of satellites randomly deployed on a sphere around Earth. Our new analysis approach characterizes the localization performance by its asymptotic behavior as the number of satellites gets large while assuming a dense network. Using the law of large numbers, we derive closed-form expressions for the asymptotic Cramér Rao bound (CRB) from which we draw valuable insights. The resulting expressions depend solely on the network statistics and are not a function of a particular network configuration. We consider two types of estimators. The first uses the exact statistical model, and hence employs both timing and amplitude information. The second estimator ignores the amplitudes and hence uses only time difference of arrival (TDOA) information. The asymptotic CRB indicates that for practical system setup, a TDOA estimator approaches the performance of the ideal estimator. For both estimators, the localization accuracy improves as satellites get closer to Earth. The latter finding is essential in light of the proliferation of low-Earth-orbit (LEO) satellites and motivates a further study of localization-performance in such networks. Besides, we show that the vertical localization accuracy is lower than the horizontal accuracy and is also more sensitive to the receiver field-of-view.

I. INTRODUCTION

Localization using satellites has long been widespread but has attracted renewed interest due to the launching of rising numbers of satellites [1–3]. Traditional global navigation satellite systems (GNSS) include the American GPS, the Russian GLONASS (e.g., [4]), the Chinese BeiDou (e.g., [5]) and the European Galileo (e.g., [6]). The current trend in GNSS utilizes multiple GNSS types to improve localization accuracy (e.g., [7]). This trend underscores the importance of studying localization accuracy with a large number of satellites. Furthermore, the recent launches of low earth orbit (LEO) communication satellites (such as OneWeb [8]) enables new alternatives for high precision localization through these satellites. Each of these constellations is expected to have thousands of satellites. This paper focuses on the characterization of localization accuracy with a large number of satellites.

In any GNSS, the user computes its position from signals transmitted by a set of visible satellites. These systems are commonly used for security, communication, surveillance, reconnaissance, traffic monitoring and other applications (e.g., [9, 10]).

State-of-the-art localization methods utilize time difference of arrival (TDOA) [11–25], frequency difference of arrival (FDOA) or both [15, 26, 27]. Localization information is

also embedded in the received signal strength (RSS) [28–32] but is generally known (and proved below) to be negligible for satellite localization. This work analyzes the asymptotic performance of a system with a large number of satellites using TDOA or TDOA+RSS. Asymptotic performance with FDOA is left for future research.

The Cramér-Rao lower bound (CRB) is an essential tool for the performance analysis of localization systems. However, in many configurations, mainly when there are many sensors, the CRB expression is complicated and hard to interpret. Moreover, an expression that depends on a specific configuration is inconvenient since satellite-network geometry varies over time.

Incorporating randomness can lead to a more informative expression, which depends solely on a few system parameters. For example, in ground based localization, Zheng et al. [33] investigated the sensor-density effect on localization performance and bounded the expected CRB for RSS-based estimation (using a non-standard attenuation model in which the signal decayed exponentially with the squared distance). Shoari and A. Seyedi [34] also treated the CRB as a random variable depending on the sensor locations. They provided closed-form lower and upper bounds on the localization performance in the presence of Rayleigh fading, using the Law of Large Numbers. Bergel and Noam [35] derived the expected CRB for Poisson point process sensor-locations, using closed-form expressions for the CRB that were derived by [36].

In this paper, we examine the case of numerous satellites and use the Law of Large Numbers to calculate the localization-accuracy asymptotic behavior, as a function of the number of satellites, for systems that employ either TDOA or TDOA+RSS localization. The analysis reveals new insights on satellite localization systems. In particular, for a given number of satellites, we show that localization accuracy is better as the satellites heights get lower, as long as we maintain sufficient coverage. We also show that the vertical localization accuracy is lower than the horizontal accuracy, and is also more sensitive to the receiver field of view.

The remainder of this paper is as follows. In Section II we formulate the problem, including the signal model, assumptions about the system and the unknown parameters. In Section III, we derive the asymptotic CRB for TDOA+RSS receiver localization in satellites. In Section IV, we derive the asymptotic performance of TDOA only receiver localization via a satellite network, and show that it is close to optimal in practical setups. The section also includes valuable insights. Simulation results appear in Section V. Section VI includes a summary and conclusions.

H. Halevi, I. Bergel and Y. Noam are with the Faculty of engineering, Bar-Ilan University, Ramat-Gan, 5290002 Israel (e-mail: hodaya.halevi.613@gmail.com; yair.noam@biu.ac.il).

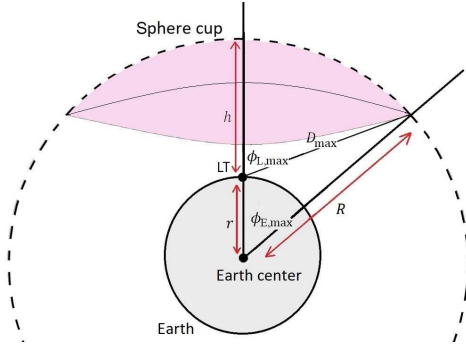


Fig. 1. System model: The satellites are randomly scattered around the Earth, and the LT can only receive from satellites located in the pink sphere cup defined by $\phi_{L,\max}$.

Notation: Bold face upper (lower) case letters denotes matrices (vectors), $[A]_{i,j}$ denotes the i, j entry of the matrix \mathbf{A} and \mathbf{A}^\top is its transpose. For brevity, we use $\sum_i(\cdot)$ for $\sum_{i=1}^N(\cdot)$.

II. SYSTEM MODEL

We consider the localization of a single land terminal (LT) at an unknown location through a network of N satellites. The satellites are uniformly distributed on a sphere of radius $R = r_e + \tilde{h}$ around the Earth, where \tilde{h} is the satellite height relative to Earth surface, and r_e is Earth radius.¹ Without loss of generality, we assume that the LT is horizontally located at the true North Pole. That is, the LT is at an elevation δ above the north pole. We also denote the distance of the LT from the Earth center by $r = r_e + \delta$. We will assume throughout that $\delta \ll r_e$ and $\delta \ll h$. Thus, in the text we will refer to r also as the Earth radius. Yet, we emphasize that the exact meaning of r (and the only way that it is used in the equations) is the LT distance from the Earth center. For mathematical simplicity, it is also convenient to work with the relative satellite height $h = \tilde{h} - \delta$ (thus, $R = r + h$ and again h is approximately equal to \tilde{h}).

We use three coordinate-systems. The first is an Earth-centered, Earth-fixed (ECEF) [38] cartesian right hinged system, used for reference and error calculation. The other two coordinate systems are spherical. One is centered at Earth center and is called the E coordinates. Here, the LT is located at the point $(r, 0, 90^\circ)$, that is, at radius r , azimuth 0 and elevation 90° , respectively, whereas satellite- m is at $(R, \theta_{E,m}, \phi_{E,m})$ where $R = r + h$.

The second spherical coordinate system is centered at the LT and is called the L coordinates. Note that azimuth is identical in both systems, $\theta_{L,m} = \theta_{E,m}$, whereas the elevation angles are not. The latter two satisfy

$$\sin \phi_{L,m} = \frac{R}{D_m} \sin \phi_{E,m}, \quad \cos \phi_{L,m} = \frac{R \cos \phi_{E,m} - r}{D_m} \quad (1)$$

¹In reality, satellite constellation design aims at maximizing coverage. Thus the probability of two satellites being near each other is typically smaller than in a uniformly distributed constellation. However, the satellite distribution is becoming more uniform as their number increases. Furthermore, in the case of multi-GNSS, the combined distribution is typically close to uniform.

where

$$\begin{aligned} D_m &= \sqrt{R^2 + r^2 - 2rR \cos \phi_{E,m}} \\ &= \sqrt{R^2 - r^2 \sin^2 \phi_{L,m} - r \cos \phi_{L,m}} \end{aligned} \quad (2)$$

is the distance between the LT and satellite- m . We assume the LT points upward (to space) and has a viewing angle $2\phi_{L,\max}$, $0 < \phi_{L,\max} < \pi/2$, as depicted in Fig. 1. We denote satellite m location by $\boldsymbol{\xi}_m = [x_m, y_m, z_m]^\top$ and collect all these points in $\boldsymbol{\xi}_1^N = [\boldsymbol{\xi}_1 \dots \boldsymbol{\xi}_N]$. Finally, we denote the unknown parameter of interest (the LT position) by $\boldsymbol{\xi} = [x, y, z]^\top$.

The signal transmission begins at time $t = T_0$, unknown to the receiver. Typically, GNSS uses Code-Division Multiple Access (CDMA) to differentiate the signals from different satellites. For simplicity, we consider Time-Division Multiple Access (TDMA), in which the same signal is transmitted by different satellites at different times. Note that the performance of TDMA and CDMA are nearly identical (e.g., [39]).

We assume that different satellites transmit with a large enough time difference so there is no inter-satellite interference and the noise is independent while receiving these signals. Without contradicting the above, we also assume that the transmission time gap between satellites is small enough such that the movement of the LT during this time is negligible. The transmission time gap between satellites is known to the LT and hence has no effect on the performance. Thus, in the following we ignore this time gap, and simply assume that the LT can receive each of the satellites signal independently of the others.

Satellite m signal as received at the LT is given by [35]

$$r_m(t) = D_m^{-1} s(t - \tau_m - T_0) \mathbf{1}_{[\phi_{L,m} < \phi_{L,\max}]} + v_m(t) \quad (3)$$

where $t \in \mathbb{R}_+$, $m \in \mathbb{N}$, $s(t)$ is a known transmitted waveform, $\mathbf{1}_{[\cdot]}$ denotes the indicator function and $v_m(t)$ is a white Gaussian noise with spectral density $N_0/2$. The propagation time delay is $\tau_m = D_m/c$, where c is the speed of light. In this paper we consider the estimation of $\boldsymbol{\xi}$ from the observations $\{r_m\}_{m=1}^N$, observed by the LT. We assume the following regularity conditions: $s(t)$ is continuous, differentiable, equals 0 for all $t \leq 0$ and there exists a non negative function $g(t)$, with $\int_0^\infty g(t)dt < \infty$, such that:

$$|s(t)|, \left| \frac{\partial s(t)}{\partial t} \right| \leq g(t) \quad \forall t. \quad (4)$$

We will show that the performance can be characterized by the signal energy $E_s \triangleq \int_{-\infty}^\infty s^2(t)dt$ and the effective bandwidth

$$W_e \triangleq \sqrt{\frac{\int_{-\infty}^\infty (\partial s(t)/\partial t)^2 dt}{\int_{-\infty}^\infty s^2(t)dt}} \quad (5)$$

Finally, we denote

$$\rho = E_s/N_0, \quad \eta = W_e^2/c^2 \quad (6)$$

and denote the received signal energy if a satellite is exactly above the receiver by $E_{s,\max} = E_s/h^2$. Note that the latter is a reference energy and does not require an actual satellite at that location.

III. ASYMPTOTIC PERFORMANCE FOR TDOA+RSS

We now derive an asymptotic expression for the CRB as the number of satellites increases. We first derive the CRB(ξ_1^N) on the estimation error of ξ as a function of the satellite locations, ξ_1^N , and then evaluate its limiting behavior as N increases. According to the Cramér-Rao theorem [40], the maximum likelihood estimator performance converges to the CRB for high enough SNR. Note that during the derivation of CRB(ξ_1^N), the satellites locations ξ_1^N are considered deterministic.

The estimation uses continuous-time signals, and hence, may exploit both TDOA and RSS information. The Fisher information matrix (FIM) for estimating γ is

$$\mathbf{J} = \sum_i \mathbf{J}_i \mathbf{1}_{\phi_{L,i}} \quad (7)$$

where \mathbf{J}_i is the matrix that represents the contribution of sensor i and given by (8), at the top of the next page (see [17]), $K_i = \frac{2\rho}{D_i^2} (1 + \eta D_i^2)$, $\mathbf{1}_{\phi_{L,i}} = \mathbf{1}_{[\phi_{L,i} < \phi_{L,\max}]}$ and $L_i = \frac{2\rho\eta}{D_i^2}$.

Let $\hat{\xi} = [\hat{x}, \hat{y}, \hat{z}]^T$ be an unbiased estimate of ξ . Here, we consider three kinds of localization errors: the overall 3D error $e_{xyz} = \|\hat{\xi} - \xi\|$, a horizontal error $e_{xy} = \sqrt{(\hat{x} - x)^2 + (\hat{y} - y)^2}$ and the altitude error $e_z = |\hat{z} - z|$. The CRB on each error is the sum of the corresponding diagonal entries of the inverse FIM. Moreover, the first CRB is equal to the sum of the two others,

$$\text{CRB}_{xyz}(\xi_1^N) = \text{CRB}_{xy}(\xi_1^N) + \text{CRB}_z(\xi_1^N) \quad (9)$$

where $\text{CRB}_{xy}(\xi_1^N) = [\mathbf{J}^{-1}]_{1,1} + [\mathbf{J}^{-1}]_{2,2}$ and $\text{CRB}_z(\xi_1^N) = [\mathbf{J}^{-1}]_{3,3}$. Recalling that the satellite-locations ξ_1^N are random, it follows that the CRB is also random. Thus, we define the following limiting expressions:

$$\begin{aligned} \text{LCRB}_{xy} &= \lim_{N \rightarrow \infty} N \cdot \text{CRB}_{xy}(\xi_1^N) \\ \text{LCRB}_z &= \lim_{N \rightarrow \infty} N \cdot \text{CRB}_z(\xi_1^N) \\ \text{LCRB}_{xyz} &= \lim_{N \rightarrow \infty} N \cdot \text{CRB}_{xyz}(\xi_1^N) \\ &= \text{LCRB}_{xy} + \text{LCRB}_z. \end{aligned} \quad (10)$$

where the limit is in the almost sure convergence sense. The following theorem expresses the first two quantities in closed form as a function of the system parameters (see Fig. 1).

Theorem 1: For the system defined in Sec. II, LCRB_{xy} , LCRB_z (10), are given by

$$\begin{aligned} \text{LCRB}_{xy} &= \frac{64Rr^3}{\rho} \left[4(2\eta(R^2 + r^2) - 1) \log\left(\frac{D_{\max}}{h}\right) \right. \\ &\quad \left. + \frac{(2(\eta(R^2 - r^2)^2 - 2(R^2 + r^2)))(h^2 - D_{\max}^2)}{D_{\max}^2 h^2} \right. \\ &\quad \left. - 4\eta r(h - D_{\max}\zeta) + \frac{(R^2 - r^2)^2 (h^4 - D_{\max}^4)}{D_{\max}^4 h^4} \right]^{-1} \quad (11) \end{aligned}$$

$$\begin{aligned} \text{LCRB}_z &= \frac{16Rr^3}{\rho} \left(2(R^2 - r^2)(\eta(R^2 - r^2) - 2) \right. \\ &\quad \left. \cdot (h^{-2} - D_{\max}^{-2}) - 4(2\eta(R^2 - r^2) - 1) \log\left(\frac{D_{\max}}{h}\right) \right. \\ &\quad \left. + 4\eta r(h - D_{\max}\zeta) + \frac{(R^2 - r^2)^2 (D_{\max}^4 - h^4)}{D_{\max}^4 h^4} \right. \\ &\quad \left. - \frac{16\eta(D_{\max}(R + r\zeta) - (R^2 - r^2))^2}{D_{\max}^2 \log\left(\frac{D_{\max}}{h}\right)} \right)^{-1} \quad (12) \end{aligned}$$

where $\zeta = \cos \phi_{L,\max}$ and

$$D_{\max} = \sqrt{R^2 + r^2(\zeta^2 - 1)} - r\zeta. \quad (13)$$

Proof: see Appendix A. ■

While (11) and (12) seem complicated, they well characterize the achievable localization accuracy for a large number of satellites. Section IV provides further insights from these expressions. Before that, the following section characterizes the performance of estimators that only utilize timing data (TDOA). Such an approach is important because (as proved below) amplitude data (RSS) contribution is negligible in satellite localization (with a reasonable transmission bandwidth).

IV. ASYMPTOTIC PERFORMANCE FOR TDOA

A. Estimation Based Solely on TDOA

An estimator that utilizes timing information while ignoring the signal strength information is, by definition, sub-optimal. Thus, its performance cannot be characterized by the CRB of the problem. Instead, we need to consider the performance of a specific estimator. To this end we consider the maximum likelihood estimator in an alternative channel model, in which the signal strength is not a function of the receiver location, by replacing the signal in (3) with

$$\tilde{r}_m(t) = A_m s(t - \tau_m - T_0) \mathbf{1}_{[\phi_{L,m} < \phi_{L,\max}]} + v_m(t). \quad (14)$$

Here, the overall unknown parameter vector is $\tilde{\gamma} = [\gamma^T, \mathbf{a}^T]^T$, where the amplitudes $\mathbf{a} = [A_1 \dots, A_N]$ are a nuisance parameter-vector. We denote the probability distribution induced by the alternative model as \tilde{P}_γ and the corresponding likelihood by $\tilde{L}(r_1 \dots r_N, \tilde{\gamma})$. In the sequel, we derive the ML estimator of $\tilde{\gamma}$ from the distribution \tilde{P}_γ . Note that the latter estimator considers the amplitudes, \mathbf{a} , as a separate parameter vector, which is not a function $\{D_m\}_{m=1}^N$, hence not a function of the RSS.

B. Mismatching

We now study the performance of the estimator derived while assuming that (14) holds while (3) is the actual signal-model. Here, the expression for the CRB under (14), dubbed mismatched CRB in this subsection, is not a lower bound on the mean square error (MSE) of every estimator. The problem of deriving estimators under a model that is not the actual

$$\mathbf{J}_i = \begin{pmatrix} K_i \sin^2 \phi_{L,i} \cos^2 \theta_i & K_i \sin^2 \phi_{L,i} \cos \theta_i \sin \theta_i & K_i \sin \phi_{L,i} \cos \theta_i \cos \phi_{L,i} & -L_i \sin \phi_{L,i} \cos \theta_i \\ K_i \sin^2 \phi_{L,i} \cos \theta_i \sin \theta_i & K_i \sin^2 \phi_{L,i} \sin^2 \theta_i & K_i \sin \phi_{L,i} \sin \theta_i \cos \phi_{L,i} & -L_i \sin \phi_{L,i} \sin \theta_i \\ K_i \sin \phi_{L,i} \cos \theta_i \cos \phi_{L,i} & K_i \sin \phi_{L,i} \sin \theta_i \cos \phi_{L,i} & K_i \cos^2 \phi_{L,i} & -L_i \cos \phi_{L,i} \\ -L_i \sin \phi_{L,i} \cos \theta_i & -L_i \sin \phi_{L,i} \sin \theta_i & -L_i \cos \phi_{L,i} & L_i \end{pmatrix} \quad (8)$$

probability distribution governing the observations is known as mismodeling. While the mismodeled CRB is not a general lower bound, it is a very useful tool if the performance of ML under mismodeling approaches it asymptotically. A sufficient condition for such a convergence is the following:

Theorem 2 ([41]): Considering an estimator that performs ML based on the likelihood $f(r(t); \boldsymbol{\theta})$ for estimating $\boldsymbol{\theta} \in \Theta$ from the observation $r(t)$, where $g(r(t))$ be the likelihood function based on the actual distribution of $r(t)$. The ML-MSE of the considered estimator approaches the CRB derived under $f(r(t); \boldsymbol{\theta})$ if there exists $\boldsymbol{\theta}_* \in \Theta$, dubbed "legal" $\boldsymbol{\theta}_*$, such that $g(r(t)) = f(r(t); \boldsymbol{\theta}_*)$.

We note that in the problem at hand, $A_{m*} = D_m^{-1}$ yields a "legal" parameter vector ($\boldsymbol{\theta}_*$). Explicitly, considering Theorem 2, the actual distribution ($g(r(t))$ in the theorem) is defined by (3) for a given value of γ , say γ_a , while the parametric family is $\tilde{L}(r_1 \dots r_N, \tilde{\gamma})$ ($f(r(t), \boldsymbol{\theta})$ in the theorem), the parametric family, $\tilde{L}(r_1, \dots, L_N, \tilde{\gamma})$ is obtained under the non-physical model in (14), but, it does include the actual likelihood. The latter is a special case of $\tilde{L}(\tilde{r}, \tilde{\gamma})$ when substituting $A_m = D_{m,*}^{-1}$ in $\tilde{\gamma}$, where $D_{m,*}$ is the actual distance between satellite- m and the LT.

Thus, the ML performance are indeed characterized by deriving the CRB for the model in (14). While using the notation \widetilde{CRB} for the CRB formula of the model (14), we remember that this is not an actual bound, and use it solely to characterize the ML performance. In the next subsection, we show that this performance is very close to the true CRB (derived in Section III) when W_e is large enough. Thus, this alternative model yields convenient, closed-form-expression for performance analysis.

The corresponding FIM for $\tilde{\gamma}$ estimation is

$$\tilde{\mathbf{J}}_{\text{extended}} = \begin{pmatrix} \tilde{\mathbf{J}} & \mathbf{J}_{\text{cross}} \\ \mathbf{J}_{\text{cross}}^H & \mathbf{J}_{\text{amp}} \end{pmatrix} \quad (15)$$

where $\mathbf{J}_{\text{amp}} = 2\rho\mathbf{I}_N$ is the FIM for estimating \mathbf{a} and $\tilde{\mathbf{J}}$ is the FIM for the estimation of γ , which we present below. Now that the amplitudes are unknown nuisance parameters, we begin with evaluating their effect on the localization error. In Appendix B, we show no coupling between the estimation of γ and the estimation of \mathbf{a} . Explicitly, $\mathbf{J}_{\text{cross}}$ is zero; hence \widetilde{CRB} for estimating γ is unchanged whether \mathbf{a} is estimated or known in advance. Henceforth, we assume that the amplitudes are known and focus on the unknown γ . Similar to \mathbf{J} (see (8)), the FIM $\tilde{\mathbf{J}}$ for estimating γ is

$$\tilde{\mathbf{J}} = \sum_i \tilde{\mathbf{J}}_i \mathbf{1}_{\phi_{L,i}} \quad (16)$$

where $\tilde{\mathbf{J}}_i$ is given by (17), at the top of the next page.

Similar to the RSS-TDOA case, we consider three kinds of estimation errors:

$$\widetilde{CRB}_{\text{xyz}}(\boldsymbol{\xi}_1^N) = \widetilde{CRB}_{\text{xy}}(\boldsymbol{\xi}_1^N) + \widetilde{CRB}_z(\boldsymbol{\xi}_1^N) \quad (18)$$

where $\widetilde{CRB}_{\text{xy}}(\boldsymbol{\xi}_1^N) = [\tilde{\mathbf{J}}^{-1}]_{1,1} + [\tilde{\mathbf{J}}^{-1}]_{2,2}$ and $\widetilde{CRB}_z(\boldsymbol{\xi}_1^N) = [\tilde{\mathbf{J}}^{-1}]_{3,3}$.

C. Asymptotic Performance Analysis

As in (10), we consider

$$\begin{aligned} \widetilde{LCRB}_{\text{xyz}} &= \lim_{N \rightarrow \infty} N \cdot \widetilde{CRB}_{\text{xyz}} \\ \widetilde{LCRB}_{\text{xy}} &= \lim_{N \rightarrow \infty} N \cdot \widetilde{CRB}_{\text{xy}} \\ \widetilde{LCRB}_z &= \lim_{N \rightarrow \infty} N \cdot \widetilde{CRB}_z. \end{aligned} \quad (19)$$

The following theorem provides closed-form expressions for the latter terms.

Theorem 3: For the system defined in Sec. II, $\widetilde{LCRB}_{\text{xy}}$, \widetilde{LCRB}_z (see (19)) are given by

$$\begin{aligned} \widetilde{LCRB}_{\text{xy}} &= \left[\eta\rho \left(\log \left(\frac{D_{\text{max}}}{h} \right) \frac{((r+h)^2 + r^2)}{8(r+h)r^3} \right. \right. \\ &\quad \left. \left. - \frac{r+h-r\zeta^2-\zeta D_{\text{max}}}{8(r+h)r^2} \right) \right]^{-1} \end{aligned} \quad (20)$$

$$\begin{aligned} \widetilde{LCRB}_z &= \left[\eta\rho \left(\frac{r+h-r\zeta^2-\zeta D_{\text{max}}}{2(r+h)r^2} \right. \right. \\ &\quad \left. \left. - \frac{h(2r+h)}{2r^3(r+h)} \log \left(\frac{D_{\text{max}}}{h} \right) \right. \right. \\ &\quad \left. \left. - \frac{[r+h-D_{\text{max}}^{-1}(r(h-D_{\text{max}}\zeta)+h(r+h))]^2}{r^3(r+h) \log(D_{\text{max}}/h)} \right) \right]^{-1} \end{aligned} \quad (21)$$

Proof: see Appendix C. ■

Although very popular [14–22, 42, 43], estimation based solely on TDOA is not optimal. In practice, however, TDOA is significantly more informative than RSS. The following lemma guarantees that RSS information is negligible for large enough bandwidth.

Lemma 4: For the system defined in Sec. II,

$$\text{CRB}_{\text{xy}} = \widetilde{CRB}_{\text{xy}} + o(W_e^{-2}) \quad (22)$$

$$\text{CRB}_z = \widetilde{CRB}_z + o(W_e^{-2}). \quad (23)$$

Proof: see Appendix D. ■

Furthermore, the \widetilde{CRB} converges to CRB when K_i approaches L_i . The latter occurs if $1 \ll \frac{D_i^2 W_e^2}{c^2}$ for every D_i .

$$\tilde{\mathbf{J}}_i = \begin{pmatrix} L_i \sin^2 \phi_{L,i} \cos^2 \theta_i & L_i \sin^2 \phi_{L,i} \cos \theta_i \sin \theta_i & L_i \sin \phi_{L,i} \cos \theta_i \cos \phi_{L,i} & -L_i \sin \phi_{L,i} \cos \theta_i \\ L_i \sin^2 \phi_{L,i} \cos \theta_i \sin \theta_i & L_i \sin^2 \phi_{L,i} \sin^2 \theta_i & L_i \sin \phi_{L,i} \sin \theta_i \cos \phi_{L,i} & -L_i \sin \phi_{L,i} \sin \theta_i \\ L_i \sin \phi_{L,i} \cos \theta_i \cos \phi_{L,i} & L_i \sin \phi_{L,i} \sin \theta_i \cos \phi_{L,i} & L_i \cos^2 \phi_{L,i} & -L_i \cos \phi_{L,i} \\ -L_i \sin \phi_{L,i} \cos \theta_i & -L_i \sin \phi_{L,i} \sin \theta_i & -L_i \cos \phi_{L,i} & L_i \end{pmatrix} \quad (17)$$

As $D_i \geq h$, we conclude that RSS information is negligible for

$$W_e \gg \frac{c}{h}. \quad (24)$$

To illustrate the latter approximation, consider a satellite at 20,000 km height. The minimal bandwidth at which (24) is satisfied is 15 Hz, where the typical bandwidth is at least one MHz. Thus, in most practical scenarios, the RSS effect on the estimation accuracy is negligible.

Now that we showed that estimation solely utilizing TDOA is near-optimal in most practical scenarios, we turn our attention to evaluating its performance. The latter analysis is even further motivated because TDOA localization is simpler than localization that also combines RSS.² Moreover, the asymptotic expression for TDOA localization-accuracy, ($\widetilde{\text{LCRB}}$), is much simpler than the asymptotic CRB (although nearly identical in practice).

For a sufficient number of satellites, Theorem 3 provides a good approximation for the localization accuracy, $\widetilde{\text{CRB}}$ (cf. (19)), as follows:

$$\begin{aligned} \widetilde{\text{CRB}}_{xy}(\xi_1^N) &\approx \widetilde{\text{ACRB}}_{xy} \triangleq \frac{\widetilde{\text{LCRB}}_{xy}}{N} \\ \widetilde{\text{CRB}}_z(\xi_1^N) &\approx \widetilde{\text{ACRB}}_z \triangleq \frac{\widetilde{\text{LCRB}}_z}{N} \end{aligned} \quad (25)$$

and combining the latter two yields the following approximated for the actual localization accuracy (see (18)). Unlike the exact $\widetilde{\text{CRB}}$, $\widetilde{\text{ACRB}}$ is not a function of a particular satellite configuration, but only of some general system parameters. Therefore, the latter can even be used for determining these parameters and enhanced performance already in the design phase before deploying such a massive constellation. More importantly, the exact $\widetilde{\text{CRB}}$ depends on the location of each of the satellites, which continually change, while the $\widetilde{\text{ACRB}}$ provides a good approximation, without considering specific satellite locations. We further demonstrate how useful $\widetilde{\text{ACRB}}$ is in the next section.

V. NUMERICAL RESULTS

We now turn to numerical analysis for further insights and to demonstrate the theory. In all simulations, unless stated otherwise, the satellites height is $h = 20000$ Km; $\eta\rho = 6.4 \cdot 10^{13}$; the LT coverage (maximal viewing) angle is $\phi_{L,\max} = 60^\circ$ (which is equivalent to $\phi_{E,\max} = 47.93^\circ$, measured from Earth's center, for satellites at $h = 20000$ Km); and Earth's radius is $r = 6371$ Km. Finally, as described in Sec. II, the satellites are uniformly distributed around the Earth.

²Hence RSS is rare in practical satellite localization.

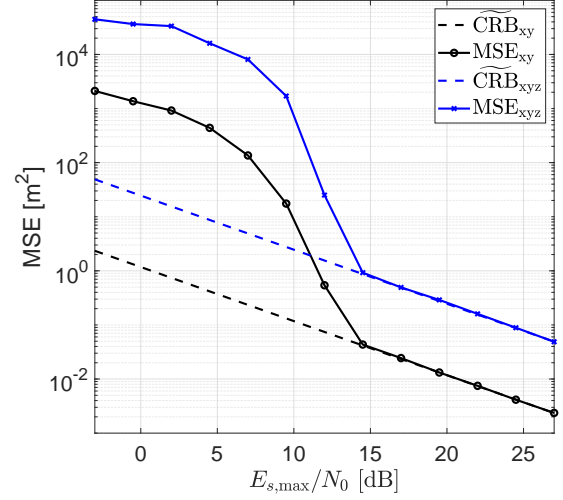


Fig. 2. MSE of the TDOA receiver localization as a function of $E_{s,\max}/N_0$, compared to the corresponding $\widetilde{\text{CRB}}$. Two models are considered separately: in the first one the z coordinate is considered known so only MSE_{xy} is examined, whereas in the second model the z coordinate is assumed to be unknown and MSE_{xyz} is examined.

A. Performance of ML Estimator

As a first step, we show that the (non asymptotic) CRB, $\widetilde{\text{CRB}}$ indeed predicts the performance of the TDOA based ML estimator. We consider the localization when one satellite is located precisely above the terminal and five more satellites are evenly distributed on the circle at elevation $\phi_L = 30^\circ$. Hence, the received energy from the central satellite is, by definition, $E_{s,\max}$, while the received energy from the other satellites is lower due to their larger distance. Following our TDOA localization approach (see Sec. IV), the terminal estimated the amplitudes and location jointly via the ML estimator based on (14). We evaluated the localization MSE by averaging the error using 1000 Monte Carlo trials and compared it to the corresponding CRB, $\widetilde{\text{CRB}}$, as a function of $E_{s,\max}/N_0$.

Fig. 2 depicts the localization error for two estimation scenarios. In the first, we assumed that the receiver knows the z coordinate, whereas, in the second, it does not, hence performing 2D and 3D TDOA-based localization, respectively. The figure presents the MSE compared to $\widetilde{\text{CRB}}_{xy}$ and $\widetilde{\text{CRB}}_{xyz}$ (see (25) and (18)), for the first and the second case, respectively. The results corroborate the well-known asymptotic efficiency of the ML estimator; i.e., beyond a threshold SNR, the estimator operates in the *small error regime* where the MSE approaches the lower bound. Moreover, as expected, 2D localization is more accurate than 3D localization. However, the factor of more than ten between the two indicates that estimating altitude (z coordinate) is challenging compared to

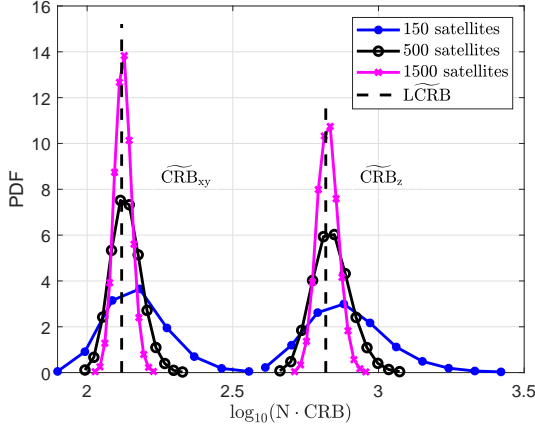


Fig. 3. PDF of $N \cdot \widehat{\text{CRB}}_{xy}$ and $N \cdot \widehat{\text{CRB}}_z$ for various numbers of satellites. The figure also shows the limit values, $\widehat{\text{LCRB}}_{xy}$ and $\widehat{\text{LCRB}}_z$ (ξ_1^N was randomly generated and CRB was calculated using ξ_1^N).

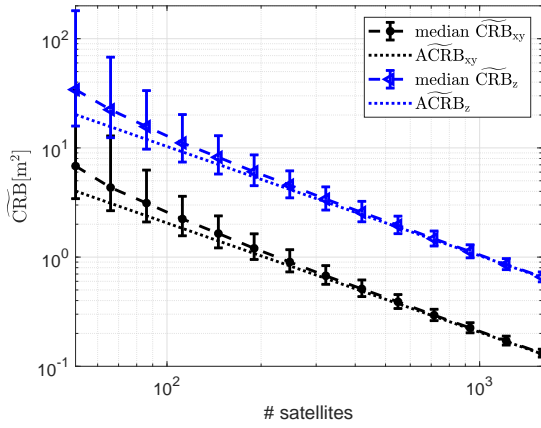


Fig. 4. Empirical median of $\widehat{\text{CRB}}_{xy}$ and $\widehat{\text{CRB}}_z$ and the respective limit values as a function of N , the number of satellites around the Earth.

horizontal localization.

B. Performance Convergence

We now study the convergence of $N \cdot \widehat{\text{CRB}}$ to the corresponding bound $\widehat{\text{LCRB}}$. Fig. 3 depicts the empirical probability density function (PDF) of $N \cdot \widehat{\text{CRB}}$ s based on 40000 random network realizations for various satellite numbers. The figure shows both the PDFs of $N \cdot \widehat{\text{CRB}}_{xy}$ and of $N \cdot \widehat{\text{CRB}}_z$, as well as the theoretical limits (20) and (21). The results demonstrate the increasing accuracy of the limiting expression as the number of satellites grows.

Fig. 4 studies the latter convergence in terms of the empirical median of the random $\widehat{\text{CRB}}$. The figure error bars (here and for all subsequent figures) mark the 10th and 90th percentiles of the $\widehat{\text{CRB}}$. For each simulation point, we used 200 Monte Carlo trials, each with an independent realization of ξ_1^N , from which we calculated $\widehat{\text{CRB}}(\xi_1^N)$. The figure shows that $\widehat{\text{CRB}}$ empirical median converges to the corresponding $\widehat{\text{ACRB}}$ as the number of satellites gets large. Recall that the strip created by the error bars encapsulates 80% of the $\widehat{\text{CRB}}$

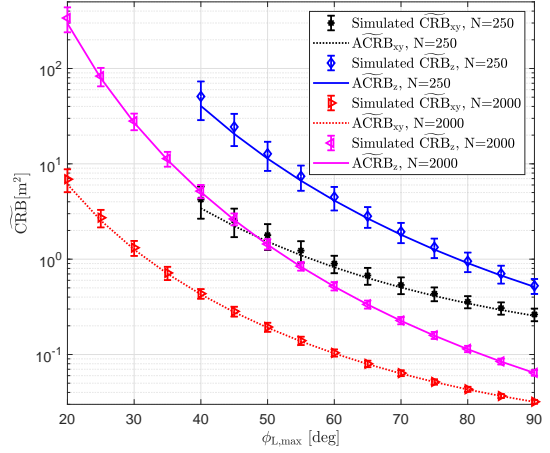


Fig. 5. Empirical median of $\widehat{\text{CRB}}_{xy}$ and $\widehat{\text{CRB}}_z$ and the respective limit values $\widehat{\text{ACRB}}_{xy}$, $\widehat{\text{ACRB}}_z$ as a function of $\phi_{L,\max}$ for $N = 250$ and $N = 2000$ satellites around Earth.

realizations. The fact that this gap is tiny for large satellite numbers demonstrates performance convergence. Furthermore, the approximation is quite good even for a relatively small number of satellites. For example, for 420 satellites, 80% of the evaluated $\widehat{\text{CRB}}_z$ were within 50% of the median and 80% of the evaluated $\widehat{\text{CRB}}_{xy}$ were within 36% of the median.

C. Height and Angle Effect and Coverage Probability

We now study the effect of h and ϕ_{\max} on the convergence rate of $\widehat{\text{CRB}}$ toward $\widehat{\text{ACRB}}$. Fig. 5 depicts the median $\widehat{\text{CRB}}$ and the $\widehat{\text{ACRB}}$ as a function of the LT coverage angle, $\phi_{L,\max}$, for 250 and 2000 satellites uniformly distributed around Earth. In all cases, increasing $\phi_{L,\max}$ reduces the $\widehat{\text{CRB}}$, implying improved estimation accuracy. The improvement is due to the increased LT coverage-angle that allows reception from more satellites. Moreover, the additional received satellites as $\phi_{L,\max}$ increases further decreases the gap between the error bars. Interestingly, the increase in $\phi_{L,\max}$ affects $\widehat{\text{CRB}}_z$ more than $\widehat{\text{CRB}}_{xy}$. The intuition behind this observation is that for small $\phi_{L,\max}$, all satellites are approximately above the terminal, thus enhancing the horizontal resolution more than the vertical one. As $\phi_{L,\max}$ increases, the receiver gets signals from different directions, thus improving its z-axis resolution.

Note that 3D TDOA localization requires at least four satellites. Consequently, besides localization-accuracy, we need to consider also the localization-identifiability; i.e., the probability of having four satellites in the LT coverage cup. To better understand the identifiability, we define the coverage probability as the probability of having four or more satellites in the LT coverage cup. The probability that a given satellite is in the coverage cup is

$$p = \frac{1 - \cos \phi_{E,\max}}{2} = \frac{h - D_{\max} \cos \phi_{L,\max}}{2R}. \quad (26)$$

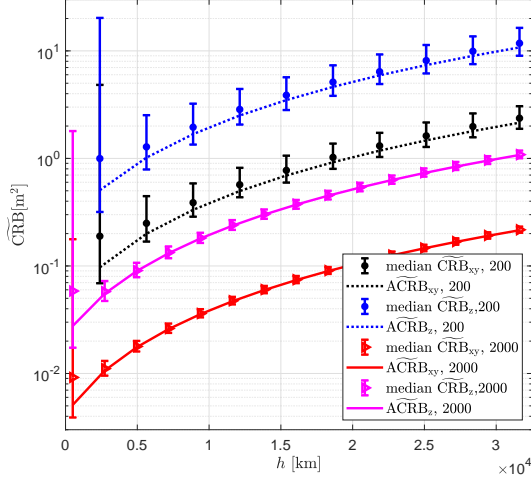


Fig. 6. Empirical median of $N \cdot \widetilde{\text{CRB}}_{xy}$ and $N \cdot \widetilde{\text{CRB}}_z$ and the respective ACRBs as a function of h . In this simulation, $N = 250$.

Recalling that the satellite locations are i.i.d., the probability for more than three satellites in the coverage cup is

$$P_{\text{cov}} = 1 - \sum_{m=0}^3 \binom{N}{m} p^m (1-p)^{N-m}. \quad (27)$$

Note that actual satellite constellation (e.g., GPS) may achieve better coverage for the same number of satellites, as explained in Footnote 1. This is achieved by careful planning of the satellites' orbits. However, the planning becomes very difficult for larger constellations, and does not hold at all for multi-GNSS localization.

From (27) one may evaluate the minimal coverage-angle guaranteeing a given coverage probability. For example, for satellites at 20 000 km height, a 90% coverage probability is achieved with $\phi_{L,\max} = 24.5^\circ$ and $\phi_{L,\max} = 8.7^\circ$ for 250 and 2000 satellites, respectively. Fig. 5 (as well as Fig. 4 and Fig. 6) only presents results for scenarios with at least 90% coverage. As the coverage probability is higher in the 2000-satellite deployment, this curve indeed starts at a smaller angle than the 250-satellite curve.

Fig. 6 depicts the empirical median of $\widetilde{\text{CRB}}$ and the corresponding limit, $\widetilde{\text{ACRB}}$, as a function of the satellites height, h . The figure considers 200 and 2000 satellites randomly scattered around Earth. Note that the number of satellites within the LT coverage cup increases as h increases (keeping $\phi_{L,\max} = 60^\circ$), but at a lower rate than in the previous figure; i.e., changing h from 5000 km to 35000 km increases the number of visible satellites by only 70%. Thus, the gap between the error bars decreases but does not disappear as h increases.

Despite the increasing number of visible satellites, the theoretical $\widetilde{\text{ACRB}}$ gets larger with h . We thus conclude that if there is a sufficient amount of satellites, they should be located as closer to Earth as possible.

However, as Fig. 6 shows, one should caution when using the latter conclusion with a finite number of satellites. If the

satellites are too low, their average number within the LT coverage cup is small, thus rendering the asymptotic analysis unsuitable. We further discuss this trade-off in the following subsection.

From (27), the minimal height ensuring a 90% coverage (which is the curves initial heights) for $\phi_{L,\max} = 60^\circ$ is 2400 km and 500 km for 200 and 2000 satellites, respectively. We, therefore, conclude that the monotonic increase of $\widetilde{\text{ACRB}}$ with the height is useful only above a height that guarantees sufficient coverage.

D. Insights Via Large and Small h Approximations.

We begin with characterizing $\widetilde{\text{ACRB}}$ for very small and very large heights.

Theorem 5: The asymptotic behavior of $\widetilde{\text{ACRB}}_{xy}$ and $\widetilde{\text{ACRB}}_z$ is described by the following limits:

$$\begin{aligned} \alpha_{xy} &\triangleq \lim_{h \rightarrow 0} \widetilde{\text{ACRB}}_{xy} \\ &= \frac{-8r^2}{\eta\rho N \left(2 \log \cos \phi_{L,\max} + \sin^2 \phi_{L,\max} \right)} \end{aligned} \quad (28)$$

$$\begin{aligned} \alpha_z &\triangleq \lim_{h \rightarrow 0} \widetilde{\text{ACRB}}_z \\ &= \frac{2r^2}{\eta\rho N \left(\sin^2 \phi_{L,\max} + \frac{2(1 - \cos \phi_{L,\max})^2}{\log \cos \phi_{L,\max}} \right)} \end{aligned} \quad (29)$$

$$\begin{aligned} \beta_{xy} &\triangleq \lim_{h \rightarrow \infty} \frac{\widetilde{\text{ACRB}}_{xy}}{h^2} \\ &= \frac{12}{\eta\rho N (\cos \phi_{L,\max} + 2)(1 - \cos \phi_{L,\max})^2} \end{aligned} \quad (30)$$

$$\beta_z \triangleq \lim_{h \rightarrow \infty} \frac{\widetilde{\text{ACRB}}_z}{h^2} = \frac{12}{\eta\rho N (1 - \cos \phi_{L,\max})^3} \quad (31)$$

Proof: see Appendix E. ■

Fig. 7 depicts the asymptotic factors of Theorem 5. We depict each α_{xy} and α_z as is, whereas, to adjust the graph units, we multiply β_{xy} and β_z by h^2 . As expected, both α and β decrease when the angle increases. Interestingly, at low angles, the α_{xy} and β_{xy} scale as ϕ^{-4} whereas the α_z and β_z scale as ϕ^{-6} . Beyond corroboration, the aforementioned observation quantifies our previous conclusion regarding the higher dependence of the vertical estimation on coverage angle.

The h^2 scaling of the ACRB calls for comment. Three factors affect the localization accuracy as the satellites' height increases. First, the received power from each satellite decreases as $1/h^2$. Because the ACRB scales as $1/E_s$, the effect of the satellite height matches the ACRB scaling exactly. The second factor is the increase in the number of observable satellites as h increases, which improves the accuracy. The third factor is a less adequate system topology (since all the transmitters are located farther away from the target), which degrades localization accuracy. The fact that the asymptotic performance scales as h^2 shows that the received energy is the dominant factor, whereas the two other factors become negligible for large heights.

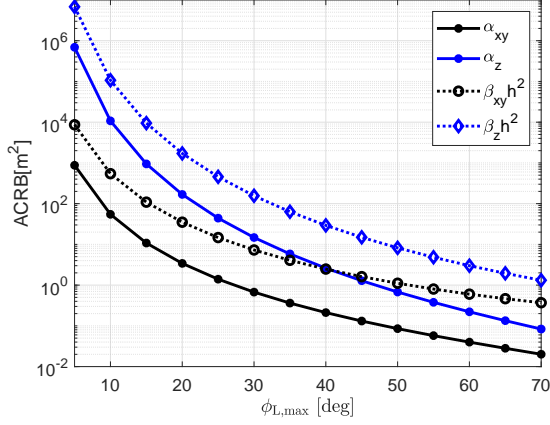


Fig. 7. Two parts of AACRB produced in Theorem 5, as a function of $\phi_{L,\max}$. $N = 200$. The AACRB_{xy} scales as ϕ^{-4} whereas the AACRB_z scales as ϕ^{-6} .

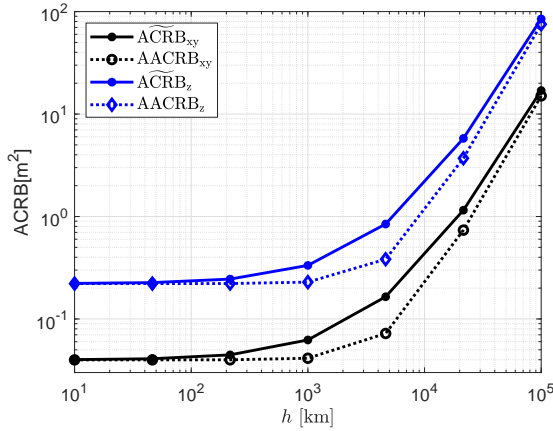


Fig. 8. $\widetilde{\text{ACRB}}$ and AACRB as a function of h for xy and z estimation.

Combining the limits from Theorem 5, we can also produce an approximated formula, which is close to $\widetilde{\text{ACRB}}$ but much simpler:

$$\text{AACRB}_{xy} = \alpha_{xy} + \beta_{xy}h^2 \quad (32)$$

$$\text{AACRB}_z = \alpha_z + \beta_zh^2 \quad (33)$$

Fig. 8 depicts the $\widetilde{\text{ACRB}}$, (25), and AACRB, (32) and (33), as a function of h , corroborating the limits. Moreover, this simple expression is a reasonable approximation for all heights. The approximation maximum deviation from the actual $\widetilde{\text{ACRB}}$ is by a factor of 2.2.

VI. CONCLUSIONS

We presented a new approach for analyzing TDOA and TDOA-RSS-based receiver localization via a satellite network. Assuming uniform distributed satellites on a sphere around the Earth, we used the Law of Large Numbers to calculate the localization-accuracy limiting-behavior. The resulting expressions depend solely on the network statistics and are not a function of a particular satellites locations. We also presented a simple condition proving that the RSS information is

negligible in practical scenarios, and that the TDOA accuracy approaches the RSS+TDOA accuracy.

Numerical results demonstrated the convergence of the actual performance to the theoretical prediction. We used these findings to study the performance expressions and to draw novel insights. In particular, we showed that the ACRB increases monotonically with the height and scales as h^2 for large h . Thus, as long as we guarantee a sufficient coverage probability, a lower satellite-height will result in better localization accuracy for any number of satellites. We also showed that the vertical localization accuracy is typically lower than the horizontal accuracy and also more sensitive to the maximal receiver antenna angle, $\phi_{L,\max}$; i.e., the vertical accuracy degrades much faster than the horizontal as the $\phi_{L,\max}$ decreases.

While the satellites are continually moving, the derived expressions depend on the network statistics and not on the specific locations. Thus, the presented closed-form-performance expressions are convenient and straightforward and can be used for a performance approximation that does not change over time. The derived expressions also provide insights on various network parameters (e.g., number of satellites, height, power), even if the actual deployment is yet unknown. Further research is necessary to better characterize the convergence-rate and its dependency on the different parameters.

APPENDIX A PROOF OF THEOREM 1

Using the definition of CRB_{xy} and CRB_z , and the continuity of $(\cdot)^{-1}$ for matrices whose determinant is bounded away from zero:

$$\begin{aligned} \text{LCRB}_{xy} &= \left[\lim_{N \rightarrow \infty} \frac{\mathbf{J}}{N} \right]_{1,1}^{-1} + \left[\lim_{N \rightarrow \infty} \frac{\mathbf{J}}{N} \right]_{2,2}^{-1} \\ \text{LCRB}_z &= \left[\lim_{N \rightarrow \infty} \frac{\mathbf{J}}{N} \right]_{3,3}^{-1}. \end{aligned} \quad (34)$$

Considering the uniform random satellite locations, each of \mathbf{J} entries is the sum of i.i.d. random variables. We thus employ the Law of Large Numbers to evaluate the expectation with respect to these locations. Explicitly, representing an entry of \mathbf{J} by $[\mathbf{J}]_{m,n} = \sum_i b_i$, we use $[\lim_{N \rightarrow \infty} \frac{\mathbf{J}}{N}]_{m,n} = \text{E}[b_i]$.

Employing the Law of Total Expectation, we first condition on all elevation angles, $\{\phi_{L,i}\}$, and then take the expectation with respect to these angles. Accordingly, the expectation of sums involving $\sin \theta$ or $\cos \theta$ is zero, whereas for sums with $\sin^2 \theta$ or $\cos^2 \theta$, it equals $\frac{1}{2}$. It follows that

$$\begin{aligned} &E \left[\frac{[\mathbf{J}]_{m,n}}{N} \mid \{\phi_{L,i}\} \right] \\ &= \begin{cases} \frac{1}{2} \text{E}[K_i \sin^2 \phi_{L,i} \mathbf{1}_{\phi_{L,i}}] & m = 1, 2, n = m \\ \text{E}[K_i \cos^2 \phi_{L,i} \mathbf{1}_{\phi_{L,i}}] & m = 3, n = 3 \\ \text{E}[L_i \cos \phi_{L,i} \mathbf{1}_{\phi_{L,i}}] & m = 3, 4, n = 7 - m \\ \text{E}[L_i \phi_{L,i} \mathbf{1}_{\phi_{L,i}}] & m = 4, n = 4 \\ 0 & \text{o.w.} \end{cases} \end{aligned} \quad (35)$$

Because $\text{E}[\mathbf{J}/N]$ is a block diagonal matrix, the block corresponding to (x, y) in $N \cdot \text{CRB}$ is the same as though (z, T_0)

were known; implying no coupling between (x, y) and (z, T_0) . From an estimation point of view, it means that knowing the unknowing (z, T_0) does not affect the estimation accuracy of (x, y) under the regime in which CRB is asymptotically tight. We now calculate LCRB_{xy} . From (35) it follows that

$$\text{LCRB}_{xy} = \frac{4}{\mathbb{E}[K_i \sin^2 \phi_{L,i} \mathbf{1}_{\phi_{L,i}}]}. \quad (36)$$

Using (1) and (2) one obtains

$$\begin{aligned} K_i \sin^2 \phi_{L,i} &= \frac{2\rho}{D_i^4} (1 + \eta D_i^2) \sin^2 \phi_{L,i} \\ &= 2\rho R^2 D_i^{-6} (1 + \eta D_i^2) \sin^2 \phi_{E,i}. \end{aligned} \quad (37)$$

Noting that $\chi \triangleq \cos \phi_{E,i}$ is uniformly distributed over $[-1, 1]$, and defining $\chi_{\max} \triangleq \cos \phi_{E,\max}$, one obtains:

$$\begin{aligned} \mathbb{E}[K_i \sin^2 \phi_{L,i} \mathbf{1}_{\phi_{L,i}}] &= \rho R^2 \int_{-1}^1 \frac{1 - \chi^2}{(R^2 + r^2 - 2rR\chi)^3} \\ &\quad \cdot (1 + \eta(R^2 + r^2 - 2rR\chi)) \mathbf{1}_{\chi \in [\chi_{\max}, 1]} d\chi \\ &= \frac{\rho}{16r^3 R} \left[4(2\eta(r^2 + R^2) - 1) \log\left(\frac{D_{\max}}{h}\right) \right. \\ &\quad \left. + \frac{(2\eta(r^2 - R^2)^2 - 4(r^2 + R^2))(h^2 - D_{\max}^2)}{D_{\max}^2 h^2} \right. \\ &\quad \left. - 4\eta r R(1 - \chi_{\max}) + \frac{(r^2 - R^2)^2 (h^4 - D_{\max}^4)}{D_{\max}^4 h^4} \right] \end{aligned} \quad (38)$$

where D_{\max} is given in (13). Substituting (1) and simplifying establishes the desired result, (11).

To derive LCRB_z , we consider the inverse of the second block in (35), which yields

$$\begin{aligned} \text{LCRB}_z &= \mathbb{E}[L_i \mathbf{1}_{\phi_{L,i}}] \cdot (\mathbb{E}[K_i \cos^2 \phi_{L,i} \mathbf{1}_{\phi_{L,i}}] \mathbb{E}[L_i \mathbf{1}_{\phi_{L,i}}] \\ &\quad - \mathbb{E}^2[L_i \cos \phi_{L,i} \mathbf{1}_{\phi_{L,i}}])^{-1}. \end{aligned} \quad (39)$$

Considering the numerator and, once again, transforming to E-coordinates one obtains

$$\begin{aligned} \mathbb{E}[L_i \mathbf{1}_{\phi_{L,i}}] &= \eta\rho \int_{-1}^1 \frac{\mathbf{1}_{\chi \in [\chi_{\max}, 1]}}{R^2 + r^2 - 2rR\chi} d\chi \\ &= \frac{\eta\rho}{rR} \log\left(\frac{D_{\max}}{h}\right). \end{aligned} \quad (40)$$

Examining the denominator of (39), the first term is given by

$$\begin{aligned} \mathbb{E}[K_i \cos^2 \phi_{L,i} \mathbf{1}_{\phi_{L,i}}] &= \mathbb{E}\left[\frac{2\rho}{D_i^4} (1 + \eta D_i^2) \cos^2 \phi_{L,i} \mathbf{1}_{\phi_{L,i}}\right] \\ &= \mathbb{E}\left[\frac{2\rho}{D_i^6} (1 + \eta D_i^2) (R \cos \phi_{E,i} - r) \mathbf{1}_{\phi_{E,i} \in [0, \phi_{\max, e}]}\right] \\ &= \frac{\rho}{16r^3 R} \left[\frac{2(r^2 - R^2)(\eta(r^2 - R^2) + 2)(D_{\max}^2 - h^2)}{h^2 D_{\max}^2} \right. \\ &\quad \left. - 4(2\eta(R^2 - r^2) - 1) \log\left(\frac{D_{\max}}{h}\right) \right. \\ &\quad \left. + 4\eta r R(1 - \chi_{\max}) + \frac{(r^2 - R^2)^2 (D_{\max}^4 - h^4)}{h^4 D_{\max}^4} \right]. \end{aligned} \quad (41)$$

Now to $\mathbb{E}[L_i \cos \phi_{L,i} \mathbf{1}_{\phi_{L,i}}]$, using (1) again:

$$\begin{aligned} \mathbb{E}[L_i \cos \phi_{L,i} \mathbf{1}_{\phi_{L,i}}] &= \mathbb{E}\left[\frac{2\eta\rho}{D_i^3} (R \cos \phi_{E,i} - r) \mathbf{1}_{\phi_{E,i}}\right] \\ &= \frac{\eta\rho}{r^2} \left(1 - \frac{R - r\chi_{\max}}{D_{\max}}\right). \end{aligned} \quad (42)$$

Combining all together and simplifying yields (12).

APPENDIX B

DECOUPLING OF \mathbf{a} AND γ

This appendix provides a proof for the following theorem:

Theorem 6: Assuming the signal model (14), there is no coupling between the γ estimation and the \mathbf{a} estimation.

Proof: To prove the theorem we show that FIM cross-entries are zero. That is, we need to prove that

$$\begin{aligned} \mathbb{E}\left[\frac{\partial^2 L(\tilde{\gamma})}{\partial A_m \partial x} | \tilde{\gamma}\right] &= \mathbb{E}\left[\frac{\partial^2 L(\tilde{\gamma})}{\partial A_m \partial y} | \tilde{\gamma}\right] = \mathbb{E}\left[\frac{\partial^2 L(\tilde{\gamma})}{\partial A_m \partial z} | \tilde{\gamma}\right] \\ &= \mathbb{E}\left[\frac{\partial^2 L(\tilde{\gamma})}{\partial A_m \partial T_0} | \tilde{\gamma}\right] = 0, \quad \forall m. \end{aligned} \quad (43)$$

The log likelihood function is given (up to an additive constant) by

$$\begin{aligned} L(\tilde{\gamma}) &= \sum_{m=1}^M \log(f(\tilde{r}_m | \tilde{\gamma})) \\ &= - \sum_{m=1}^M \frac{1}{N_0} \int_0^\infty (\tilde{r}_m(t) - A_m s(t - \tau_m(\tilde{\gamma})))^2 dt \end{aligned} \quad (44)$$

where $\tau_m(\tilde{\gamma}) = \frac{D_m(\tilde{\gamma})}{c} + T_0$. To obtain the cross entries, we differentiate (45) with respect to (w.r.t.) A_m and then w.r.t. the location or the time coordinate. The log likelihood derivative w.r.t. A_m is

$$\begin{aligned} \frac{\partial L(\tilde{\gamma})}{\partial A_m} &= \frac{2}{N_0} \int_0^\infty s(t - \tau_m(\tilde{\gamma})) \tilde{r}_m(t) dt \\ &\quad - \frac{2}{N_0} \int_0^\infty A_m s^2(t - \tau_m(\tilde{\gamma})) dt. \end{aligned} \quad (45)$$

Now, examining the cross entries corresponding to T_0 and A_m , the derivative of (45) w.r.t. T_0 is

$$\begin{aligned} \frac{\partial^2 L(\tilde{\gamma})}{\partial A_m \partial T_0} &= -\frac{2}{N_0} \int_0^\infty \dot{s}(t - \tau_m(\tilde{\gamma})) \tilde{r}_m(t) dt \\ &\quad + \frac{4}{N_0} \int_0^\infty A_m s(t - \tau_m(\tilde{\gamma})) \dot{s}(t - \tau_m(\tilde{\gamma})) dt \\ &= -\frac{2}{N_0} \int_0^\infty \dot{s}(t - \tau_m(\tilde{\gamma})) [\tilde{r}_m(t) - 2A_m s(t - \tau_m(\tilde{\gamma}))] dt. \end{aligned} \quad (46)$$

Noting that $\mathbb{E}[\tilde{r}_m(t)] = A_m s(t - \tau_m(\tilde{\gamma}))$ and

$$\int_0^\infty s(t) \dot{s}(t) dt = 0 \quad (47)$$

it follows that

$$\mathbb{E}\left[\frac{\partial^2 L(\tilde{\gamma})}{\partial A_m \partial T_0} | \tilde{\gamma}\right] = \frac{2A_m}{N_0} \int_0^\infty \dot{s}(t - \tau_m(\tilde{\gamma})) s(t - \tau_m(\tilde{\gamma})) dt = 0. \quad (48)$$

Next, to the cross entries corresponding to x and A_m . The parameter x affects the likelihood via D_m . Since we use

TDOA while ignoring RSS, only $\tau_m(\tilde{\gamma})$ is a function of D_m . Further deriving (45) w.r.t. x , we obtain (49), from which (50) follows:

$$\begin{aligned} \frac{\partial^2 L(\tilde{\gamma})}{\partial A_m \partial x} &= -\frac{2}{cN_0} \int_0^\infty \dot{s}(t - \tau_m(\tilde{\gamma})) \tilde{r}_m(t) \sin \phi_{E,m} \cos \theta_{E,m} dt \\ &+ \frac{4}{cN_0} \int_0^\infty A_m s(t - \tau_m(\tilde{\gamma})) \dot{s}(t - \tau_m(\tilde{\gamma})) \sin \phi_{E,m} \cos \theta_{E,m} dt \\ &= -\frac{2 \sin \phi_{E,m} \cos \theta_{E,m}}{cN_0} \\ &\int_0^\infty \dot{s}(t - \tau_m(\tilde{\gamma})) [\tilde{r}_m(t) - 2A_m s(t - \tau_m(\tilde{\gamma}))] dt \quad (49) \end{aligned}$$

$$\begin{aligned} \mathbb{E} \left[\frac{\partial^2 L(\tilde{\gamma})}{\partial A_m \partial x} \Big| \tilde{\gamma} \right] &= \frac{2 \sin \phi_{E,m} \cos \theta_{E,m}}{cN_0} \\ &\int_0^\infty \dot{s}(t - \tau_m(\tilde{\gamma})) A_m s(t - \tau_m(\tilde{\gamma})) dt = 0 \end{aligned} \quad (50)$$

The proof for the cross elements corresponding to the y - and z -coordinates follow exactly the same reasoning as (49) and (50). ■

APPENDIX C PROOF OF THEOREM 3

Following the same approach as in Appendix A, we have that

$$\begin{aligned} \widetilde{\text{LCRB}}_{xy} &= \mathbb{E}[[\mathbf{J}]_{11}/N]^{-1} + \mathbb{E}[[\mathbf{J}]_{22}/N]^{-1} \\ \widetilde{\text{LCRB}}_z &= \mathbb{E}[[\mathbf{J}]_{33}/N]^{-1}. \end{aligned} \quad (51)$$

Using again, the Law of Total Expectation, we first consider the expectation of the FIM (17) w.r.t. to θ .

$$\begin{aligned} \mathbb{E} \left[\frac{[\mathbf{J}]_{m,n}}{N} \Big| \{\phi_{L,i}\} \right] &= \begin{cases} \frac{1}{2} \mathbb{E}[L_i \sin^2 \phi_{L,i} \mathbf{1}_{\phi_{L,i}}] & m = 1, 2, n = m \\ \mathbb{E}[L_i \cos^2 \phi_{L,i} \mathbf{1}_{\phi_{L,i}}] & m = 3, n = 3 \\ \mathbb{E}[L_i \cos \phi_{L,i} \mathbf{1}_{\phi_{L,i}}] & m = 3, 4, n = 7 - m \\ \mathbb{E}[L_i \phi_{L,i} \mathbf{1}_{\phi_{L,i}}] & m = 4, n = 4 \\ 0 & \text{o.w.} \end{cases} \quad (52) \end{aligned}$$

Beginning with $\widetilde{\text{LCRB}}_{xy}$, it follows from (52) that

$$\widetilde{\text{LCRB}}_{xy} = \frac{4}{\mathbb{E}[L_i \sin^2 \phi_{L,i} \mathbf{1}_{\phi_{L,i}}]} \quad (53)$$

and as in (38), one obtains

$$\begin{aligned} \mathbb{E} [L_i \sin^2 \phi_{L,i} \mathbf{1}_{\phi_{L,i}}] &= \mathbb{E} \left[\frac{2\rho\eta}{D_i^2} \left(\frac{R}{D_i} \sin \phi_{E,i} \right)^2 \mathbf{1}_{\phi_{E,i}} \right] \\ &= 2\rho\eta \left(\log \left(\frac{D_{\max}}{h} \right) \frac{((r+h)^2 + r^2)}{4r^3(r+h)} \right. \\ &\quad \left. - \frac{(1 - \chi_{\max})(D_{\max}^2 + r(r+h)(1 + \chi_{\max}))}{4r^2 D_{\max}^2} \right). \end{aligned} \quad (54)$$

Finally, by transforming the polar angle back to L-coordinates using Equation (1), the desired result follows.

We now derive $\widetilde{\text{LCRB}}_z$. From (52) one obtains

$$\begin{aligned} \widetilde{\text{LCRB}}_z &= \mathbb{E}[L_i \mathbf{1}_{\phi_{L,i}}] \cdot \left(\mathbb{E}[L_i \cos^2 \phi_{L,i} \mathbf{1}_{\phi_{L,i}}] \mathbb{E}[L_i] \right. \\ &\quad \left. - \mathbb{E}^2[L_i \cos \phi_{L,i} \mathbf{1}_{\phi_{L,i}}] \right)^{-1} \end{aligned} \quad (55)$$

We already evaluated all the expectations in (55) in the proof of Theorem 1, except of $\mathbb{E}[L_i \cos \phi_{L,i} \mathbf{1}_{\phi_{L,i}}]$. The latter is given by

$$\begin{aligned} \mathbb{E}[L_i \cos \phi_{L,i} \mathbf{1}_{\phi_{L,i}}] &= 2\rho\eta \mathbb{E}[D_i^{-3} (R \cos \phi_{E,i} - r) \mathbf{1}_{\phi_{E,i}}] \\ &= 2\rho\eta \frac{1 + D_{\max}^{-1} (r(\chi_{\max} - 1) - h)}{2r^2} \\ &= 2\rho\eta \frac{D_{\max}(r+h) - r(h - D_{\max}\zeta) - (r+h)h}{2(r+h)D_{\max}r^2} \\ &= 2\rho\eta \frac{D_{\max}(r(1+\zeta) + h) - 2rh - h^2}{2(r+h)D_{\max}r^2} \end{aligned} \quad (56)$$

where $\zeta = \cos \phi_{L,\max}$. Substituting all terms back in (55) establishes (21).

APPENDIX D PROOF OF LEMMA 4

Comparing (17) to (8), it follows that

$$\mathbf{J} = \tilde{\mathbf{J}} + o(W_e). \quad (57)$$

From [44], Section 5.8, it follows that:

$$\|\mathbf{J}^{-1} - \tilde{\mathbf{J}}^{-1}\| = o(W_e^{-2}). \quad (58)$$

which leads to (22) and (23).

APPENDIX E PROOF OF THEOREM 5

A. The Limit of $\widetilde{\text{ACRB}}_{xy}$ as h approaches 0

Using a second order Taylor expansion, one obtains

$$D_{\max} = \frac{h}{\zeta} - h^2 \frac{1 - \zeta^2}{2r\zeta^3} + o(h^2). \quad (59)$$

It therefore follows that

$$\lim_{h \rightarrow 0} \frac{D_{\max}}{h} = \frac{1}{\zeta} \quad (60)$$

and

$$h - D_{\max}\zeta = h^2 \frac{1 - \zeta^2}{2r\zeta^2} + o(h^2). \quad (61)$$

Using some arithmetic manipulations on (20), we can write:

$$\begin{aligned} \widetilde{\text{ACRB}}_{xy} &= 4(r+h) \cdot \left(\rho\eta N \left(\log \left(\frac{D_{\max}}{h} \right) \frac{(r+h)^2 + r^2}{2r^3} \right. \right. \\ &\quad \left. \left. - \frac{h - D_{\max}\zeta}{2r^2 D_{\max}^2} ((r+h)^2 + r(r+h - D_{\max}\zeta)) \right) \right)^{-1}. \end{aligned} \quad (62)$$

Substituting (61), one obtains:

$$\begin{aligned} \widetilde{\text{ACRB}}_{xy} &= 4(r+h) \cdot \left(\rho\eta N \left(\log \left(\frac{D_{\max}}{h} \right) \frac{(r+h)^2 + r^2}{2r^3} \right. \right. \\ &\quad \left. \left. - \frac{h^2(1-\zeta^2)}{4r^3 D_{\max}^2 \zeta^2} \left((r+h)^2 + r^2 + \frac{h^2(1-\zeta^2)}{2\zeta^2} \right. \right. \right. \\ &\quad \left. \left. \left. + o(h^2) \right) \right) \right)^{-1}. \end{aligned} \quad (63)$$

Evaluating the limit as $h \rightarrow 0$, using the continuity of $\widetilde{\text{ACRB}}_{xy}$ and (60), we get

$$\begin{aligned} \alpha_{xy} &= \lim_{h \rightarrow 0} \widetilde{\text{ACRB}}_{xy} \\ &= \frac{4r}{\rho\eta N \left(-\log(\zeta) \frac{r^2+r^2}{2r^3} - \frac{1-\zeta^2}{4r^3} (r^2+r^2) \right)}. \end{aligned} \quad (64)$$

Reorganizing this expression and substituting $\zeta = \cos \phi_{L,\max}$ completes the proof of (28).

B. The Limit of $\widetilde{\text{ACRB}}_z$ as h approaches 0

From (21) and (25), the $\widetilde{\text{ACRB}}_z$ is given by:

$$\begin{aligned} \widetilde{\text{ACRB}}_z &= \left[\eta\rho N \left(\frac{r+h-r\zeta^2-\zeta D_{\max}}{2(r+h)r^2} \right. \right. \\ &\quad \left. \left. - \frac{h(2r+h)}{2r^3(r+h)} \log \left(\frac{D_{\max}}{h} \right) \right. \right. \\ &\quad \left. \left. - \frac{(r+h-D_{\max}^{-1}(r(h-D_{\max}\zeta)+h(r+h)))^2}{r^3(r+h) \log(D_{\max}/h)} \right) \right]^{-1}. \end{aligned} \quad (65)$$

Using (61), we have

$$\begin{aligned} \widetilde{\text{ACRB}}_z &= \left[\eta\hat{r} N \left(\frac{r-r\zeta^2+h^2\frac{1-\zeta^2}{2r\zeta^2}+o(h^2)}{2(r+h)r^2} \right. \right. \\ &\quad \left. \left. - \frac{h(2r+h)}{2r^3(r+h)} \log \left(\frac{D_{\max}}{h} \right) \right. \right. \\ &\quad \left. \left. - \frac{(r+h-D_{\max}^{-1}(h^2\frac{1-\zeta^2}{2\zeta^2}+o(h^2)+h(r+h)))^2}{r^3(r+h) \log(D_{\max}/h)} \right) \right]^{-1}. \end{aligned} \quad (66)$$

We then substitute (60) and $h=0$ and get:

$$\alpha_z = \lim_{h \rightarrow 0} \widetilde{\text{ACRB}}_z = \left[\eta\rho N \left(\frac{r-r\zeta^2}{2r^3} + \frac{[r-\zeta r]^2}{r^4 \log(\zeta)} \right) \right]^{-1} \quad (67)$$

which directly leads to (29).

C. The Limit of $\widetilde{\text{ACRB}}_{xy}$ as h approaches Infinity

Evaluating the asymptotic behavior of $\log \left(\frac{D_{\max}}{h} \right)$ and $\sqrt{h^2+2hr+r^2\zeta^2}$ we have:

$$\begin{aligned} \log \left(\frac{D_{\max}}{h} \right) &= -\frac{r(\zeta-1)}{h} + \frac{r^2(\zeta-1)}{h^2} \\ &\quad + \frac{r^3(\zeta^3-9\zeta+8)}{6h^3} + o(h^{-3}) \\ &= \frac{r(\zeta-1)}{6h^3} (-6h^2+6hr+r^2\zeta(\zeta+1)-8r^2) \end{aligned} \quad (68)$$

$$\begin{aligned} \sqrt{h^2+2hr+r^2\zeta^2} &= \frac{-r^4(\zeta^4-6\zeta^2+5)}{8h^3} - \frac{r^3(\zeta^2-1)}{2h^2} \\ &\quad + \frac{r^2(\zeta^2-1)}{2h} + h+r+o(h^{-3}). \end{aligned} \quad (69)$$

Substituting the latter two into $\widetilde{\text{ACRB}}_{xy}$ and reorganizing yields:

$$\begin{aligned} \widetilde{\text{ACRB}}_{xy} &= \frac{4r^3(h+r)}{\rho\eta N} \cdot \left(\frac{r((h+r)^2+r^2)(\zeta-1)}{6h^3} \right. \\ &\quad \cdot (-6h^2+6hr+r^2\zeta(\zeta+1)-8r^2) \\ &\quad \left. + r\zeta \left(\frac{r^2(\zeta^2-1)}{2h} + h+r \right) - r(h+r) + o(h^{-1}) \right)^{-1} \\ &= \frac{12r^3h^3(h+r)}{\rho\eta N h^2 r^3 (1-\zeta)^2 (\zeta+2) + o(h^2)}. \end{aligned} \quad (70)$$

Dividing the $\widetilde{\text{ACRB}}_{xy}$ by h^2 and taking the limit, one obtains

$$\lim_{h \rightarrow \infty} \frac{\widetilde{\text{ACRB}}_{xy}}{h^2} = \frac{12}{\rho\eta N (\zeta+2)(1-\zeta)^2} \quad (71)$$

D. The Limit of $\widetilde{\text{ACRB}}_z$ as h approaches Infinity

Substituting (68) and (69) in (65) and reorganizing, we get:

$$\begin{aligned} \widetilde{\text{ACRB}}_z &= \left[\eta\rho N \left((r+h-\zeta \left(\frac{-r^4(\zeta^4-6\zeta^2+5)}{8h^3} \right. \right. \right. \\ &\quad \left. \left. + \frac{r^2(\zeta^2-1)}{2h} + h+r) \right) - \frac{r^3(\zeta^2-1)}{2h^2} \cdot (2(r+h)r^2)^{-1} \right. \\ &\quad \left. + \frac{h(2r+h)}{2r^3(r+h)} \left(\frac{6r(\zeta-1)(h^2-6hr-r^2(\zeta^2+\zeta-8))}{6h^3} \right) \right. \\ &\quad \left. + \left(2h^2+r \left(r(\zeta^2-1) + \frac{r^4(\zeta^4-6\zeta^2+5)}{4h^3} \right) \right. \right. \\ &\quad \left. \left. + \frac{r^3(\zeta^2-1)}{h^2} - \frac{r^2(\zeta^2-1)}{h} - 2h \right) \right) \right. \\ &\quad \cdot \left((r+h) \left(\frac{6r^4(\zeta-1)(h^2-6hr-r^2(\zeta^2+\zeta-8))}{6h^3} \right) \right)^{-1} \\ &\quad \left. - \left(2h \left(\frac{-r^4(\zeta^4-6\zeta^2+5)}{8h^3} - \frac{r^3(\zeta^2-1)}{2h^2} + \frac{r^2(\zeta^2-1)}{2h} \right. \right. \right. \\ &\quad \left. \left. + h-r \right) \right) \cdot \left((r+h) \right. \\ &\quad \left. \left. \cdot \frac{6r^4(\zeta-1)(h^2-6hr-r^2(\zeta^2+\zeta-8))}{6h^3} \right) \right)^{-1} \right]^{-1} \end{aligned}$$

$$= \left[96h^3(h+r)(6h^2 - 6hr - (\zeta^2 + \zeta - 8)r^2) \right. \\ \cdot \left[\rho\eta N(\zeta - 1) \left(4hr^3(\zeta - 1)(7\zeta^3 + 30\zeta^2 - 15\zeta - 166) \right. \right. \\ \left. \left. - 48h^3(\zeta^2 + 7\zeta - 14)r - 48h^4(\zeta - 1)^2 \right. \right. \\ \left. \left. + 3(\zeta + 1)(\zeta^2 - 5)(\zeta^3 + \zeta^2 + \zeta - 15)r^4 \right. \right. \\ \left. \left. - 4h^2(\zeta - 1)(\zeta + 5)(\zeta^2 + 7\zeta - 26)r^2) \right]^{-1} + o(h^{-2}). \quad (72)$$

Dividing by h^2 and taking the limit, we immediately get:

$$\lim_{h \rightarrow \infty} \frac{\widetilde{\text{ACRB}}_z}{h^2} = \frac{12}{\rho\eta N(1 - \zeta)^3} \quad (73)$$

REFERENCES

- [1] K. Jaldehag, C. Rieck, and P. Jarlemark, "Evaluation of CG-GTTS time transfer software using multiple GNSS constellations," in *2018 European Frequency and Time Forum (EFTF)*, pp. 159–166, IEEE, 2018.
- [2] X. Li, F. Ma, X. Li, H. Lv, L. Bian, Z. Jiang, and X. Zhang, "LEO constellation-augmented multi-GNSS for rapid PPP convergence," *Journal of Geodesy*, vol. 93, no. 5, pp. 749–764, 2019.
- [3] O. Montenbruck, P. Steigenberger, L. Prange, Z. Deng, Q. Zhao, F. Perosanz, I. Romero, C. Noll, A. Stürze, G. Weber, et al., "The multi-GNSS experiment (MGEX) of the international GNSS service (IGS)—achievements, prospects and challenges," *Advances in space research*, vol. 59, no. 7, pp. 1671–1697, 2017.
- [4] A. Leick, "GLONASS satellite surveying," *Journal of surveying engineering*, vol. 124, no. 2, pp. 91–99, 1998.
- [5] G. Sun and Z.-m. Ding, "Working method improvements of beidou satellite system," *Acta Electronica Sinica*, vol. 29, no. 9, pp. 1217–1220, 2001.
- [6] P. Closas, C. Fernandez-Prades, and J. A. Fernandez-Rubio, "Cramér–Rao bound analysis of positioning approaches in GNSS receivers," *IEEE Transactions on Signal Processing*, vol. 57, no. 10, pp. 3775–3786, 2009.
- [7] X. Li, M. Ge, X. Dai, X. Ren, M. Fritsche, J. Wickert, and H. Schuh, "Accuracy and reliability of multi-GNSS real-time precise positioning: GPS, GLONASS, BeiDou, and Galileo," *Journal of Geodesy*, vol. 89, no. 6, pp. 607–635, 2015.
- [8] P. B. De Selding, "Virgin, qualcomm invest in oneWeb satellite internet venture," *Space News*, vol. 15, 2015.
- [9] R. Klemm, *Applications of space-time adaptive processing*, vol. 14. IET, 2004.
- [10] H. Runge, S. Suchandt, A. Kotenkov, G. Palubinskas, U. Steinbrecher, and D. Wehling, "Traffic monitoring with TerraSAR-X," 2008.
- [11] X. Ouyang, Q. Wan, J. Cao, J. Xiong, and Q. He, "Direct TDOA geolocation of multiple frequency-hopping emitters in flat fading channels," *IET Signal Processing*, vol. 11, no. 1, pp. 80–85, 2017.
- [12] Y. Sun, K. Ho, and Q. Wan, "Solution and analysis of TDOA localization of a near or distant source in closed form," *IEEE Transactions on Signal Processing*, vol. 67, no. 2, pp. 320–335, 2018.
- [13] S. Cao, X. Chen, X. Zhang, and X. Chen, "Combined weighted method for TDOA-based localization," *IEEE Transactions on Instrumentation and Measurement*, vol. 69, no. 5, pp. 1962–1971, 2019.
- [14] C. Knapp and G. Carter, "The generalized correlation method for estimation of time delay," *IEEE transactions on acoustics, speech, and signal processing*, vol. 24, no. 4, pp. 320–327, 1976.
- [15] K. Yang, L. Jiang, and Z.-Q. Luo, "Efficient semidefinite relaxation for robust geolocation of unknown emitter by a satellite cluster using TDOA and FDOA measurements," in *2011 IEEE International Conference on Acoustics, Speech and Signal Processing (ICASSP)*, pp. 2584–2587, IEEE, 2011.
- [16] K. Yang, G. Wang, and Z.-Q. Luo, "Efficient convex relaxation methods for robust target localization by a sensor network using time differences of arrivals," *IEEE transactions on signal processing*, vol. 57, no. 7, pp. 2775–2784, 2009.
- [17] L. Mailaender, "On the geolocation bounds for round-trip time-of-arrival and all non-line-of-sight channels," *EURASIP Journal on Advances in Signal Processing*, vol. 2008, p. 37, 2008.
- [18] J. Shen, A. F. Molisch, and J. Salmi, "Accurate passive location estimation using TOA measurements," *IEEE Transactions on Wireless Communications*, vol. 11, pp. 2182–2192, Jun. 2012.
- [19] A. J. Weiss, "On the accuracy of a cellular location system based on RSS measurements," *IEEE transactions on vehicular technology*, vol. 52, no. 6, pp. 1508–1518, 2003.
- [20] I. Guvenc and C. C. Chong, "A survey on TOA based wireless localization and NLOS mitigation techniques," *IEEE Commun. Surveys Tuts.*, vol. 11, pp. 107–124, Jul.-Sep. 2009.
- [21] L. Cong and Z. Weihua, "Non-line-of-sight error mitigation in TDOA mobile location," *GLOBECOM'01. IEEE Global Telecommunications Conference (Cat. No. 01CH37270)*, vol. 1, 2001.
- [22] H. L. Van Trees and K. L. Bell, "Bayesian bounds for parameter estimation and nonlinear filtering/tracking," *AMC*, vol. 10, p. 12, 2007.
- [23] K. Ho and Y. Chan, "Solution and performance analysis of geolocation by TDOA," *IEEE Transactions on Aerospace and Electronic Systems*, vol. 29, no. 4, pp. 1311–1322, 1993.
- [24] J. A. Bhatti, T. E. Humphreys, and B. M. Ledvina, "Development and demonstration of a TDOA-based GNSS interference signal localization system," in *Proceedings of the 2012 IEEE/ION Position, Location and Navigation Symposium*, pp. 455–469, IEEE, 2012.
- [25] E. Cetin, R. J. Thompson, and A. G. Dempster, "Passive interference localization within the GNSS environmental monitoring system (GEMS): TDOA aspects," *GPS solutions*, vol. 18, no. 4, pp. 483–495, 2014.
- [26] J. Zhao, L. Li, and Y. Gong, "Joint navigation and synchronization in LEO dual-satellite geolocation systems," in *2017 IEEE 85th Vehicular Technology Conference (VTC Spring)*, pp. 1–5, IEEE, 2017.
- [27] T. Pattison and S. Chou, "Sensitivity analysis of dual-satellite geolocation," *IEEE Transactions on Aerospace and Electronic Systems*, vol. 36, no. 1, pp. 56–71, 2000.
- [28] F. M. Ghannouchi, D. Wang, and S. Tiwari, "Accurate wireless indoor position estimation by using hybrid TDOA/RSS algorithm," in *2012 IEEE International Conference on Vehicular Electronics and Safety (ICVES 2012)*, pp. 437–441, IEEE, 2012.
- [29] D. Zhu and K. Yi, "EKF localization based on TDOA/RSS in underground mines using uwb ranging," in *2011 IEEE International Conference on Signal Processing, Communications and Computing (ICSPCC)*, pp. 1–4, IEEE, 2011.
- [30] E. Kazikli and S. Gezici, "Hybrid TDOA/RSS based localization for visible light systems," *Digital Signal Processing*, vol. 86, pp. 19–28, 2019.
- [31] A. Catovic and Z. Sahinoglu, "Hybrid TOA/RSS and TDOA/RSS location estimation schemes for short-range wireless networks," *Bechtel Telecommunication Technical Journal (BTTJ)*, vol. 2, no. 2, pp. 77–84, 2004.
- [32] A. Catovic and Z. Sahinoglu, "The Cramer-Rao bounds of hybrid TOA/RSS and TDOA/RSS location estimation schemes," *IEEE Communications Letters*, vol. 8, no. 10, pp. 626–628, 2004.
- [33] Y. Zheng, R. Niu, and P. K. Varshney, "Closed-form performance for location estimation based on quantized data in sensor networks," in *2010 13th International Conference on Information Fusion*, pp. 1–7, IEEE, 2010.
- [34] A. Shoari and A. Seyedi, "Target localization with binary observations: Effect of censoring non-detecting sensors," in

- 2011 *IEEE International Symposium on Information Theory Proceedings*, pp. 2504–2508, IEEE, 2011.
- [35] I. Bergel and Y. Noam, “Lower bound on the localization error in infinite networks with random sensor locations,” *IEEE Transactions on Signal Processing*, vol. 66, pp. 1228–1241, Mar. 2018.
- [36] B. T. Sieskul, F. Zheng, and T. Kaiser, “A hybrid SS–ToA wireless NLoS geolocation based on path attenuation: ToA estimation and CRB for mobile position estimation,” *IEEE transactions on vehicular technology*, vol. 58, no. 9, pp. 4930–4942, 2009.
- [37] C. H. Gierull, D. Cerutti-Maori, and J. Ender, “Ground moving target indication with tandem satellite constellations,” *IEEE Geoscience and Remote Sensing Letters*, vol. 5, no. 4, pp. 710–714, 2008.
- [38] J. R. Clynch, “Earth coordinates,” *Electronic Documentation*, February, 2006.
- [39] C. Botteron, A. Host-Madsen, and M. Fattouche, “Cramer-rao bounds for the estimation of multipath parameters and mobiles’ positions in asynchronous DS-CDMA systems,” *IEEE Transactions on Signal Processing*, vol. 52, no. 4, pp. 862–875, 2004.
- [40] C. R. Rao, “Information and the accuracy attainable in the estimation of statistical parameters,” *Reson. J. Sci. Educ*, vol. 20, pp. 78–90, 1945.
- [41] H. White, “Maximum likelihood estimation of misspecified models,” *Econometrica: Journal of the Econometric Society*, pp. 1–25, 1982.
- [42] B. Hamon and E. Hannan, “Spectral estimation of time delay for dispersive and non-dispersive systems,” *Journal of the Royal Statistical Society: Series C (Applied Statistics)*, vol. 23, no. 2, pp. 134–142, 1974.
- [43] E. Hannan and P. Thomson, “Estimating group delay,” *Biometrika*, vol. 60, no. 2, pp. 241–253, 1973.
- [44] C. R. Johnson and R. A. Horn, *Matrix analysis*. Cambridge university press Cambridge, 1985.